NUCL SCI TECH (2019) 30:70
https://doi.org/10.1007/s41365-019-0598-y

Theoretical analyses of chemical bonding in terminal $ESThF_2$ (E = O, S, Se, Te)

Yan-Li Li[1,2] · **Xiao-Gen Xiong**[3] · **Hong-Tao Liu**[1]

Received: 9 October 2018 / Revised: 20 December 2018 / Accepted: 21 December 2018 / Published online: 9 April 2019

Abstract Analyses of chemical bonding and geometric structures in species with chalcogen elements $EThF_2$ (E = O, S, Se, Te) are performed by the density functional theory. Kohn–Sham molecular orbitals and Th–E bond lengths of these species both indicate multiple bond character for the terminal chalcogen complexes. This is also confirmed by natural bond orbital analyses using the one-electron density matrix generated by relativistic density functional calculations. Theoretical analyses indicate that electron donation from E to Th increases down the chalcogen group (O $<$ S $<$ Se $<$ Te). These molecules can serve as examples of multiple bonding between actinide elements and selenium or tellurium.

Keywords $EThF_2$ · Chemical bonding · Natural bond orbital (NBO)

1 Introduction

Terminal metal oxo ligands are considered particularly valuable intermediates in various biochemical and chemical reactions [1]. Intensive research has been conducted to probe their properties and design synthesis routes, especially complexes including late transition metal elements, which will provide a comprehensive understanding of their effects in related catalytic reactions. Owing to the important role of terminal oxo complexes in transition metal chemistry, their corresponding actinide analogs have attracted immense attention for application to thorium compounds in catalytic reactions [2]. Chemical bonding in complexes of thorium with nitrogen and oxygen is primarily ionic; therefore, it would be interesting to study the potential covalent character of the chemical bonding of actinides with heavy and soft chalcogens [3–12]. This will shed light on our knowledge of chemical bonding in compounds containing f elements, as chemical bonding between actinide elements and ligands is the current frontier of f-element research [16]. Apart from the theoretical importance, the study of actinide compounds containing soft chalcogen elements (S, Se, and Te) is important in the nuclear fuel cycle; further, soft ligands are believed to be efficient for the separation of later actinides from lanthanides [6, 11, 12, 14–17]. Anion photoelectron spectroscopy (PES) is a reliable and powerful approach to study the electronic structures of gas-phase compounds and solid materials. The spectra obtained from anion PES directly reflect the fingerprints of neutral molecules, which are formed from the detachment of electrons from anions. Hence, it would be interesting to study—both the structures of anionic and neutral complexes—and analyze the variation in electronic structures and chemical bonding during

---

This work was supported by “Strategic Priority Research Program” of the Chinese Academy of Sciences (No. XDA02020000) and the National Natural Science Foundation of China (Nos. 21573273, 21501189). Hong-Tao Liu gratefully appreciates the support from Hundred Talents Program (CAS).

✉ Hong-Tao Liu
liuhongtao@sinap.ac.cn

[1] Shanghai Institute of Applied Physics, Chinese Academy of Sciences, Shanghai 201800, China

[2] University of Chinese Academy of Sciences, Beijing 100049, China

[3] Sino-French Institute of Nuclear Engineering and Technology, Sun Yat-Sen University, Zhuhai 519082, China

electron detachment. We report an analysis of the geometric structures and chemical bonding for $EThF_2$ and $EThF_2^-$ (E = O, S, Se, Te). We also perform natural bond orbital (NBO) analyses of the bonding for $EThF_2$ and ThE with E = O, S, Se, and Te, and our theoretical results suggest a highly polarized multiple bond character of Th–E bonds.

2 Computational methods

Geometric parameters of the studied molecules were optimized using the Gaussian 09 program with the different functionals B3LYP, PBE [18], PBE0, TPSS, and TPSSh. Vibrational frequencies were also set at the same level to verify that the obtained geometries are at the minima of the potential energy surfaces. ECP60MDF [19] and the relevant basis set cc-pVTZ-PP [20] were applied for Th to consider the scalar relativistic (SR) effects. We used aug-cc-pVTZ [21] for O, F, and S and aug-cc-pVTZ-PP [22] for Se and Te, because the PBE exchange-correlation functional performs reasonably well for transition metals and even for actinide complexes [23]. Specifically, our previous work demonstrates the good performance of the PBE functional for the analysis of chemical bonding in thorium oxides [24, 25]; hence, we expect that the PBE exchange-correlation functional will be suitable for studying the molecules in this work. The PBE exchange-correlation functional executed through the ADF 2017.106 package [26] was used to optimize the geometries. The Slater basis sets of TZ2P [27] were adopted with frozen core approximation applied to the inner shells [$1s^2$–$5d^{10}$] for Th and [$1s^2$] for O. Quasi-relativistic zero-order-regular approximation (ZORA) was adopted to address the SR effects. Vibrational frequency calculations at the SR-ZORA level were implemented to confirm the real minima on the potential energy surfaces. The unrestricted Kohn–Sham approach of density functional theory (DFT) implemented in ADF was used to study the anions. The one-electron density matrix generated from ADF calculations was used to perform the NBO analyses [28].

3 Geometries and orbital analyses

3.1 Geometries

The optimized geometries and calculated frequencies for $EThF_2^-$ and $EThF_2$ at the SR-ZORA PBE/TZ2P level in comparison with previously reported values are provided in Tables 1 and 2. All the studied anion and neutral molecules possess the Cs symmetry with a $^1A'$ ground state for neutral molecules and $^2A'$ ground state for anions. Our calculated data are in accordance with previous values, suggesting that the PBE exchange-correlation functional is suitable to analyze the current species. Single-point energy calculations through CCSD(T) in the Molpro 2012.1 package [35] using the optimized geometric structures at the B3LYP level for both anions and neutrals are performed to determine the electron affinity (EA) of the studied neutral molecules. The EA values for $OThF_2$, $SThF_2$, $SeThF_2$, and $TeThF_2$ are 1.20 eV, 1.59 eV, 1.66 eV, and 1.96 eV, respectively. The calculated geometries and frequencies under the Gaussian 09/DFT level are provided in the supplementary information. The bond length of Th–E increases along the series from $OThF_2$ to $TeThF_2$ both in the anion and neutral molecules, while the bond length of Th–F exhibits an opposite trend. The calculated results also indicate a decrease in the bond angles and bond lengths from the anions to the corresponding neutral molecules, which can be attributed to singly occupied molecular orbitals (SOMOs) of the anions possessing non-negligible anti-bonding character. The calculated bond length of Th–O in the $OThF_2$ neutral molecule is 1.895 Å, which is slightly longer than the previously reported result of 1.886 Å [10] at the B3LYP level; therefore, it would be meaningful to study the properties of different functionals in complexes including the thorium atom. Ours as well as the previously calculated bond length of Th–O bond are similar in value for the ThO triple bond length (1.89 Å) obtained from atomic radii [36]. Our recent calculated bond lengths at the SR-ZORA PBE/TZ2P level for Th–S, Th–Se, and Th–Te in $SThF_2$, $SeThF_2$, and $TeThF_2$ neutral molecules are 2.423 Å, 2.583 Å, and 2.821 Å, respectively; these are higher than the calculated bond lengths of di-atomic molecules ThS ($^1\Sigma^+$, 2.343 Å), ThSe ($^1\Sigma^+$, 2.495 Å), and ThTe ($^1\Sigma^+$, 2.731 Å) at the same level. Moreover, the calculated bond lengths of Th–F in $EThF_2$ are all greater than that in ThF_2, as shown in Table 3.

Table 1 Optimized geometric parameters and calculated frequencies for $EThF_2^-$ (E = O, S, Se, Te). The data are obtained from SR-ZORA PBE/TZ2P calculations

	$OThF_2^-$	$SThF_2^-$	$SeThF_2^-$	$TeThF_2^-$
R(Th–E) (Å)	1.932	2.495	2.655	2.907
R(Th–F) (Å)	2.201	2.166	2.158	2.149
∠(EThF) (°)	112.4	115.8	117.0	119.1
∠(FThF) (°)	110.7	116.5	118.4	120.7
Th–E str.	765.0	388.5	249.2	186.6
Sym. F–Th–F	463.1	488.9	491.1	497.5
Antisym. F–Th–F	436.6	465.1	471.7	480.9

Table 2 Optimized geometric parameters and calculated frequencies for $EThF_2$ (E = O, S, Se, Te) compared to previously reported values. The data are obtained from SR-ZORA PBE/TZ2P calculations

	$OThF_2$	$SThF_2$	$SeThF_2$	$TeThF_2$
R(Th–E) (Å)	1.895, 1.886[b]	2.423	2.583	2.821
R(Th–F) (Å)	2.141, 2.157[b]	2.105	2.096	2.089
∠(EThF) (°)	110.8	107.2	107.1	107.3
∠(FThF) (°)	103.6, 107.0[b]	104.7	104.7	104.7
Th–E str.	821.0, 806.6[a], 825.9[b]	433.9	280.9	214.2
Sym. F–Th–F	532.0, 511.1[a], 513.1[b]	559.4	561.6	566.7
Antisym. F–Th–F	500.1, 482.3[a], 484.6[b]	527.3	533.1	540.0

[a] Experimental data from Ref. 10

[b] Theoretical data from Ref. 10

Table 3 Optimized geometries and calculated frequencies for ThE (E = O, S, Se, Te) and ThF_2 compared to previously reported values. The data are obtained from SR-ZORA PBE/TZ2P calculations

	R(Th–E) (Å)			Th–E str.		
	Current	Previous		Current	Previous	
	Calc.	Exp.	Calc.	Calc.	Exp.	Calc.
ThO	1.848	1.840[a]	1.846[a], 1.845[b]	894.5	895[c]	895.5[b]
ThS	2.343		2.3556[d], 2.363[e], 2.349[f]	480.7	479(1)[e], 474.7[f]	478.7[d], 477[e], 481.4[f]
ThSe	2.495		2.500[g]	307.4		306.0[g]
ThTe	2.731			229.5		
ThF_2	2.056		2.061[h]	589.4(a1)	575.1(b1)[h], 575.9(b1)[h], 583.6(b1)[i], 582.7(b1)[i]	585.4(a1)[h]
				581.2(b1)		573.4(b1)[h]

[a] Ref. 29

[b] Ref. 30

[c] Ref. 24

[d] Ref. 11

[e] Ref. 31

[f] Ref. 32

[g] Ref. 12

[h] Ref. 33

[i] Ref. 34

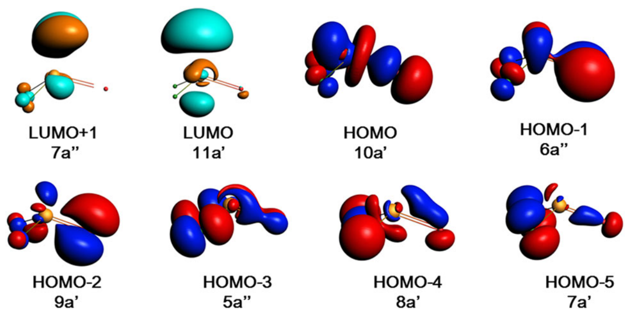

Fig. 1 (Color online) Contour plots of Kohn–Sham MOs of $OThF_2$ (isosurf = 0.05 a.u)

3.2 Orbital analyses

Figure 1 shows the contour plots of the Kohn–Sham MOs of $OThF_2$. The correlation diagram is presented in Fig. 2. The $10a'$ molecular orbital, which is the highest occupied molecular orbital (HOMO), mainly stems from O $2p$ atomic orbitals (AOs), with modest contributions from Th $6d$ and $5f$ AOs, indicating a σ bond between Th and O. The O $2p$ AOs mixed with Th $6d$ and $5f$ AOs, resulting in a weak π bonding $6a''$ (HOMO-1) molecular orbital. HOMO-2 ($9a'$) is another π orbital arising from the interactions of the $2p$ AO of oxygen with $6d$ and $5f$ AOs of thorium. Hence, the Kohn–Sham MO analysis suggests that the Th–O bond has two weak π bonds and one σ bond in the $OThF_2$ molecule, which is nearly same as the bonds in other

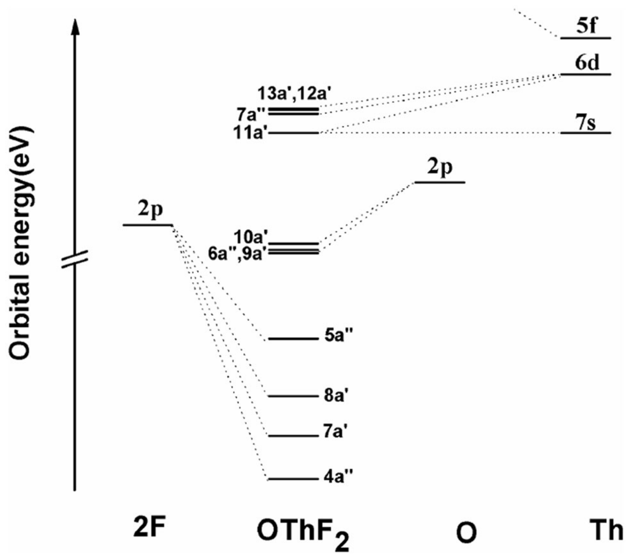

Fig. 2 Qualitative molecular orbital energy level diagram of OThF$_2$. The energy of atomic orbitals was shifted up with 6.21 eV

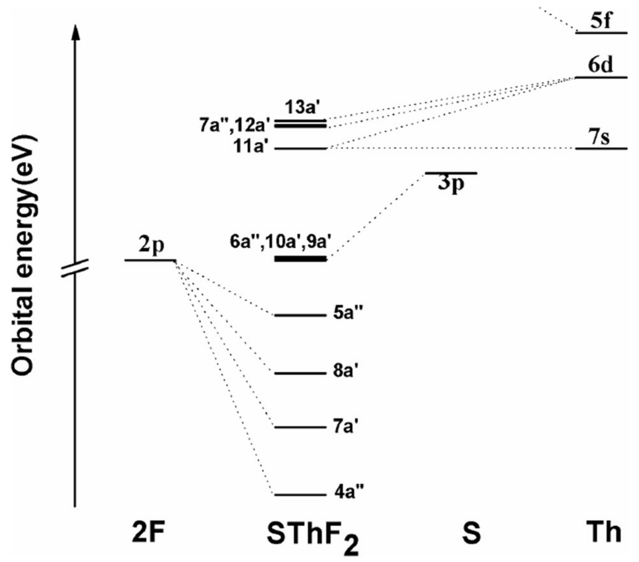

Fig. 4 Qualitative molecular orbital energy level diagram of SThF$_2$. The energy of atomic orbitals was shifted up with 5.87 eV

terminal thorium chalcogens included complexes. [13–15] NBO studies provide additional proof for the existence of multiple bonding in OThF$_2$. As displayed in Table 5, there are three bonding orbitals between Th and O, where the oxygen atom (mainly 2*p* atomic orbital (AO)) devotes around 84% to the Th–O bond; the rest originates from the mixing of Th 5*f* and 6*d* AOs, with more contribution from 6*d* orbitals than 5*f* orbitals. Because fluorine has high electronegativity, it is supposed that the AOs of oxygen would prefer to overlap more with the thorium AOs.

Figure 3 shows the contour plots of the Kohn–Sham MOs of SThF$_2$, and the correlation diagram is presented in Fig. 4. The 6a$''$ (HOMO) molecular orbital is largely composed of S 3*p* AOs, Th 6d_π AOs and a bit Th 5*f* AOs, suggesting a weak π bond between Th and S. The 3*p* AO of S interacts with 5*f*–6*d* hybridized AOs of Th, forming a weak π bonding 10a$'$ (HOMO-1) molecular orbital. Moreover, a weak σ bonding 9a$'$ (HOMO-2) molecular orbital is formed between Th and S through the overlap between 6*d* AO of Th and 3*p* AO of S; thus, identical to Th–O, Th–S shows two weak π bonds and a σ bond in SThF$_2$.

Figure 5 shows the contour plots of the Kohn–Sham MOs of SeThF$_2$, and the correlation diagram is presented in Fig. 6. Of which, 6a$''$ (HOMO) and 10a$'$ (HOMO-1) are molecular orbitals of two weak π bonds, mainly composed of 4*p* of Se and 6*d* of Th, in addition to a trace of Th-5*f* AOs. The interaction between 4*p* of Se and 6*d* of Th forms a weak σ bonding 9a$'$ (HOMO-2) molecular orbital; thus, as in the previous two cases, we suggest the Th–Se bond possess two weak π bonds and a σ bond in the SeThF$_2$ molecule.

The contour plots of the Kohn–Sham MOs of TeThF$_2$ and the correlated diagram are presented in Figs. 7 and 8, respectively. TeThF$_2$ has a bonding nature similar to the previous three molecules, and Th–Te bond possess two weak π bonds and one σ bond in the TeThF$_2$ molecule. Similarly, multiple bonding in the SThF$_2$, SeThF$_2$, and TeThF$_2$ molecules can be observed through NBO research.

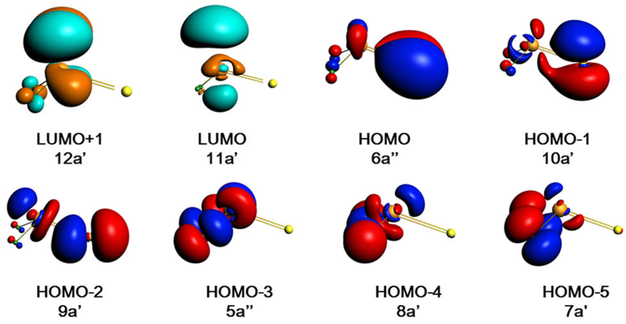

Fig. 3 (Color online) Contour plots of Kohn–Sham MOs of SThF$_2$ (isosurf = 0.05 a.u)

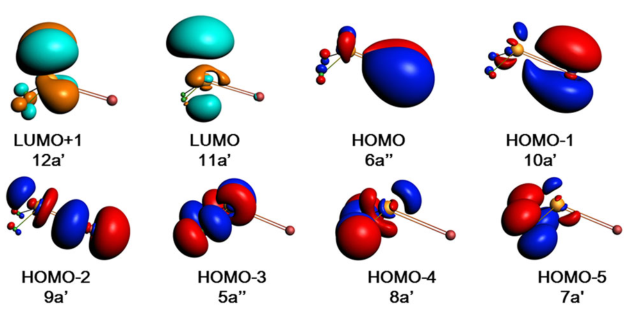

Fig. 5 (Color online) Contour plots of Kohn–Sham MOs of SeThF$_2$ (isosurf. = 0.05 a.u)

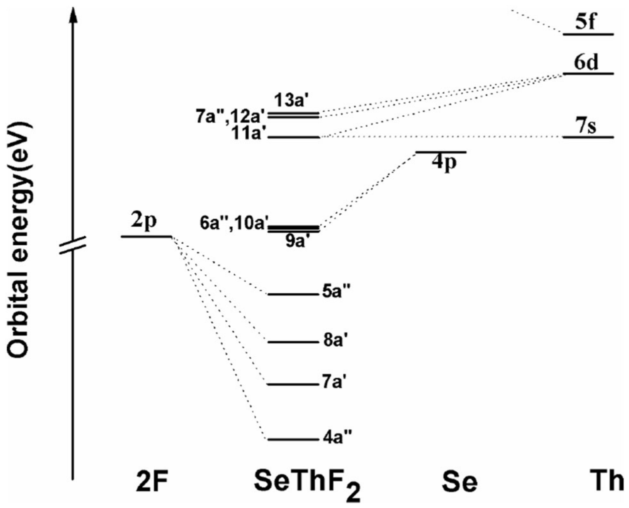

Fig. 6 Qualitative Kohn–Sham molecular orbital energy level diagram of SeThF$_2$. The energy of atomic orbitals was shifted up with 5.78 eV

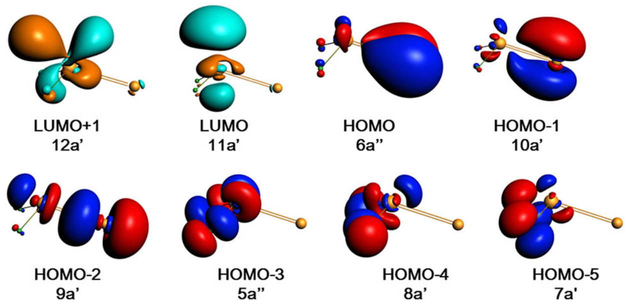

Fig. 7 (Color online) Contour plots of Kohn–Sham MOs of TeThF$_2$ (isosurf = 0.05 a.u)

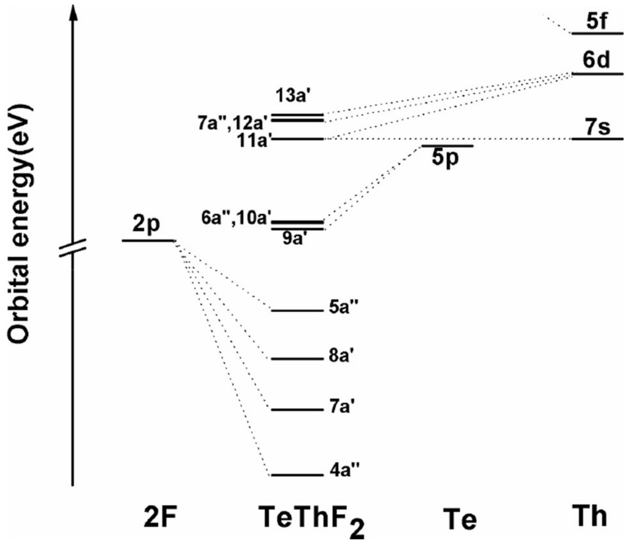

Fig. 8 Qualitative Kohn–Sham molecular orbital energy level diagram of TeThF$_2$. The energy of atomic orbitals was shifted up with 5.67 eV

As displayed in Table 5, three Th–S, Th–Se, or Th–Te bonding orbitals exist, in which the sulfur (mainly 3*p* AO), selenium (mainly 4*p* AO), or tellurium atom (mainly 5*p* AO) contributes more than 80% to the Th–S, Th–Se, or Th–Te chemical bond, respectively. Moreover, the remaining contributions are mainly attributed to the mixing of Th 5*f* and 6*d* AOs. Furthermore, the 5a$''$ (HOMO-3) and 8a$'$ (HOMO-4) molecular orbitals are mainly composed of F-2*p* AOs with detectable contribution from Th-6*d* AOs, based on Figs. 1, 3, 5 and 7, suggesting there exists head-on interplay between the AOs of fluoride and thorium atoms. However, the interaction of Th and F is essentially weak for overpowering dedication from F-2*p* AOs; therefore, the effective bond order between Th and F atoms in these complexes could be viewed as less than one, as shown in Table 8.

The relevant NBO computational results for the OThF$_2$–TeThF$_2$ are compared with those for ThO–ThTe, as listed in Tables 4, 5 and 6. Table 4 shows the increment of Th-6*d* populations and the decrement of Th-5*f* population along both the series from OThF$_2$ to TeThF$_2$ and from ThO to ThTe, respectively. Moreover, the 6*d* and 5*f* population values in EThF$_2$ are higher than those in the corresponding ThE. A highly polarized multiple bond character for all Th–E bonds in EThF$_2$ and ThE can be observed from the NBO analyses. The multiple bonds have a significant contribution from Th in the Th–S, Th–Se, and Th–Te bonds as compared with the that in the Th–O bond, where both the π and σ bonds have the same trends, suggesting a weaker covalency of the Th–O chemical bond compared to its counterparts, which is in accordance with the decrease in electronegativity from O to Te. From OThF$_2$–TeThF$_2$ and ThO–ThTe, decreasing *f* character and increasing *d* character are observed in the Th–E chemical bonds; this trend is in accordance with the natural electron population in Th-6*d* AO and Th-5*f* AO. With the addition of two F atoms, the natural electron charges on the Th center in EThF$_2$ (E = O, S, Se, Te) becomes more positive than those in ThE (E = O, S, Se, Te) because of the strong electronegativity of F, thus forming a higher oxidation state of Th. Furthermore, natural electron charges on the Th center decrease from 2.45 to 2.16 along the series of EThF$_2$, which is consistent with the decreased donation from Th to E down the chalcogen group in the order O < S < Se < Te.

Furthermore, we performed the theoretical bond analyses of EThF$_2$ and EThF$_2^-$ (E = O, S, Se, Te), as displayed in Tables 7 and 8. Generally, the bond orders of Th–E and Th–F in OThF$_2$ are slightly lower than those in EThF$_2$ (E = S, Se, Te), in which the latter species have nearly the same bond order; the same trend occurs in EThF$_2^-$ (E = O, S, Se, Te). Moreover, the bond orders of Th–E and Th–F in anions are lower than those in the corresponding neutral

Table 4 Natural electron configuration of Th atom and natural charges on Th, E (E = O, S, Se, Te), and F atoms in different molecules computed at range-separated PBE/TZ2P level through ADF

	ThO	ThS	ThSe	ThTe	$OThF_2$	$SThF_2$	$SeThF_2$	$TeThF_2$
7*s*	1.85[a], 1.84[b]	1.83, 1.80[b]	1.81, 1.79[b]	1.77	0.04	0.11	0.14	0.20
6*d*	0.68[a], 0.71[b]	1.09, 1.18[b]	1.17, 1.29[b]	1.31	1.01	1.25	1.26	1.25
5*f*	0.31[a], 0.34[b]	0.23, 0.24[b]	0.20, 0.21[b]	0.16	0.48	0.44	0.42	0.39
7*p*	0.05[a], 0.10[b]	0.03, 0.06[b]	0.04, 0.06[b]	0.05	0.01	0.01	0.01	0.02
q(Th)	1.18[a], 1.10[b]	0.85, 0.77[b]	0.81, 0.68[b]	0.73	2.54	2.22	2.20	2.16
q(E)	− 1.18[a], − 1.10[b]	− 0.85, − 0.77[b]	− 0.81, − 0.68[b]	− 0.73	− 1.11	− 0.86	− 0.85	− 0.81
q(F)					− 0.71	− 0.68	− 0.68	− 0.68

[a] Ref. 25

[b] Ref. 12

Table 5 Calculated NBO analysis of $EThF_2$ (E = O, S, Se, Te) at range-separated PBE/TZ2P level through ADF

		Th%7*s*	Th%6*d*	Th%5*f*	Th%7*p*	E%*s*	E%*p*
$OThF_2$	Th–O π	0.06	9.82	5.36	0.08	7.93	76.32
	Th–O π		7.20	5.08	0.01		87.39
	Th–O σ	0.12	10.23	5.90	0.23	11.24	71.76
$SThF_2$	Th–S π	0.04	13.15	4.41	0.26	0.81	81.11
	Th–S π		11.41	4.75	0.18		83.45
	Th–S σ	3.77	16.30	2.94	0.06	13.69	62.97
$SeThF_2$	Th–Se π	0.13	13.38	4.07	0.31	0.99	80.86
	Th–Se π		11.52	4.53	0.20		83.52
	Th–Se σ	5.28	16.21	2.36	0.01	10.63	65.19
$TeThF_2$	Th–Te π	0.85	13.21	3.41	0.53	2.43	79.36
	Th–Te π		11.55	4.17	0.29		83.80
	Th–Te σ	7.12	16.62	2.04	0.08	7.56	66.30

Table 6 Calculated NBO analysis of ThE (E = O, S, Se, Te) at range-separated PBE/TZ2P level through ADF

		Th%7*s*	Th%6*d*	Th%5*f*	Th%7*p*	M%*s*	E%*p*
ThO	Th–O π		7.89	3.90			87.97
	Th–O π		7.89	3.90			87.97
	Th–O σ	0.50	11.33	6.78	0.18	15.62	65.18
ThS	Th–S π		13.12	3.38	0.29		82.93
	Th–S π		13.12	3.38	0.29		82.93
	Th–S σ	2.03	18.22	4.26	0.01	13.64	61.44
ThSe	Th–Se π		14.03	0.03	0.34		82.22
	Th–Se π		14.03	0.03	0.34		82.22
	Th–Se σ	2.35	19.12	3.43	0.04	11.45	63.06
ThTe	Th–Te π		15.27	2.69	0.55		81.23
	Th–Te π		15.27	2.69	0.55		81.23
	Th–Te σ	3.47	20.78	2.53	0.18	10.55	61.95

species, suggesting that the extra electron undermines the interaction between Th and E (E = O, S, Se, Te) as well as Th and F and that the SOMO of anions or the lowest unoccupied molecular orbital (LUMO) of the neutral molecules exhibit a non-negligible anti-bonding character, which are in accordance with the downward trend of bond lengths from the anions to the corresponding neutral ones.

Table 7 Calculated bond orders between Th and E in EThF$_2$ and EThF$_2^-$ (E = O, S, Se, Te), the data are obtained from SR-ZORA PBE/TZ2P calculations

	OThF$_2$	OThF$_2^-$	SThF$_2$	SThF$_2^-$	SeThF$_2$	SeThF$_2^-$	TeThF$_2$	TeThF$_2^-$
Mayer	1.82	0.88	2.24	1.04	2.10	0.92	2.24	1.00
N–M	2.27	2.47	2.37	2.49	2.37	2.48	2.37	2.42
G–J	1.58	1.67	1.85	1.72	1.87	1.69	1.93	1.57
Wiberg	1.52	1.34	1.81	1.50	1.83	1.47	1.86	1.39

Table 8 Calculated bond orders between Th and F atoms in EThF$_2$ and EThF$_2^-$ (E = O, S, Se, Te), the data are obtained from SR-ZORA PBE/TZ2P calculations

	OThF$_2$	OThF$_2^-$	SThF$_2$	SThF$_2^-$	SeThF$_2$	SeThF$_2^-$	TeThF$_2$	TeThF$_2^-$
Mayer	0.54	0.13	0.58	0.19	0.58	0.22	0.59	0.29
N–M	1.03	1.04	1.04	1.05	1.04	1.05	1.04	1.06
G–J	0.67	0.62	0.70	0.64	0.70	0.64	0.71	0.62
Wiberg	0.54	0.45	0.60	0.51	0.60	0.52	0.60	0.50

4 Summary

Theoretical calculations have been carried out to investigate the species of EThF$_2$ and EThF$_2^-$ (E = O, S, Se, Te). Moreover, geometric and bonding analyses have also been conducted. The bond length of Th–E (E = O, S, Se, Te) increases and that of Th–F decreases from OThF$_2$ to TeThF$_2$. Furthermore, the bond angle of ∠EThF decreases, whereas that of ∠FThF increases from OThF$_2$ to TeThF$_2$. The bond covalency of Th–E (E = O, S, Se, Te) increases along the series from OThF$_2$ to TeThF$_2$ as the bond length of Th–F decreases. Kohn–Sham molecular orbital analyses and NBO calculation have been applied to understand the chemical bonding of Th–E and Th–F in these complexes. Our theoretical results revealed the multiple bond character of Th–E from OThF$_2$ to TeThF$_2$ in EThF$_2$ (E = O, S, Se, Te).

References

1. A. Gunay, K.H. Theopold, C−H bond activations by metal oxo compounds. Chem. Rev. **110**, 1060–1081 (2010). https://doi.org/10.1021/cr900269x
2. E. Barnea, M.S. Eisen, Organoactinides in catalysis. Coord. Chem. Rev. **250**, 855–899 (2006). https://doi.org/10.1016/j.ccr.2005.12.007
3. A.J. Gaunt, B.L. Scott, M.P. Neu, A molecular actinide–tellurium bond and comparison of bonding in [M^{III}{N(TeP*i*Pr$_2$)$_2$}$_3$] (M = U, La)*. Angew. Chem. Int. Ed. **45**, 1638–1641 (2006). https://doi.org/10.1002/anie.200503372
4. C.Z. Wang, T. Bo, J.H. Lan et al., Ultrastable actinide endohedral borospherenes. Chem. Commun. **54**, 2248–2251 (2018). https://doi.org/10.1039/c7cc09837e
5. Q.Y. Wu, Z.P. Cheng, J.H. Lan et al., Insight into the nature of M–C bonding in the lanthanide/actinide-biscarbene complexes: a theoretical perspective†. Dalton Trans. **47**, 12718–12725 (2018). https://doi.org/10.1039/c8dt02702a
6. D.E. Smiles, G. Wu, P. Hrobárik et al., Use of ^{77}Se and ^{125}Te NMR spectroscopy to probe covalency of the actinide-chalcogen bonding in [Th(En){N(SiMe$_3$)$_2$}$_3$]$^-$ (E = Se, Te; *n* = 1, 2) and their oxo-uranium (VI) congeners. J. Am. Chem. Soc. **138**, 814–825 (2016). https://doi.org/10.1021/jacs.5b07767
7. M. Ringgold, D. Rehe, P. Hrobárik et al., Thorium cubanes-synthesis, solid-state and solution structures, thermolysis, and chalcogen exchange reactions. Inorg. Chem. **57**, 7129–7141 (2018). https://doi.org/10.1021/acs.inorgchem.8b00836
8. P. Hrobárik, M. Straka, P. Pyykkö, Computational study of bonding trends in the metalloactinyl series EThM and MThM' (E = N$^-$, O, F$^+$; M, M' = Ir$^-$, Pt, Au$^+$). Chem. Phys. Lett. **431**, 6–12 (2006). https://doi.org/10.1016/j.cplett.2006.08.144
9. E.A. Pedrick, P. Hrobarik, L.A. Seaman et al., Synthesis, structure and bonding of hexaphenyl thorium(IV): observation of a non-octahedral structure. Chem. Commun. **52**, 689–692 (2016). https://doi.org/10.1039/c5cc08265j
10. Y. Gong, X.F. Wang, L. Andrews et al., Infrared spectroscopic and theoretical investigations of the OUF$_2$ and OThF$_2$ molecules with triple oxo bond character. Inorg. Chem. **51**(12), 6983–6991 (2012). https://doi.org/10.1021/ic3009128
11. X.F. Wang, L. Andrews, K.S. Thanthiriwatte et al., Infrared spectra of H$_2$ThS and H$_2$US in noble gas matrixes: enhanced H–An–S covalent bonding. Inorg. Chem. **52**, 10275–10285 (2013). https://doi.org/10.1021/ic400560k
12. T. Vent-Schmidt, L. Andrews, K.S. Thanthiriwatte et al., Reaction of laser-ablated uranium and thorium atoms with H$_2$Se: a rare example of selenium multiple bonding. Inorg. Chem. **54**, 9761–9769 (2015). https://doi.org/10.1021/acs.inorgchem.5b01383
13. R.G. Denning, Electronic structure and bonding in actinyl ions and their analogs. J. Phys. Chem. A **111**(20), 4125–4143 (2007). https://doi.org/10.1021/jp071061n
14. M.P. Jensen, A.H. Bond, Comparison of covalency in the complexes of trivalent actinide and lanthanide cations. J. Am. Chem. Soc. **124**(33), 9870–9877 (2002). https://doi.org/10.1021/ja0178620
15. M.P. Jensen, A.H. Bond, Influence of aggregation on the extraction of trivalent lanthanide and actinide cations by purified Cyanex 272, Cyanex 301, and Cyanex 302. Radiochim. Acta **90**(4), 205–209 (2002). https://doi.org/10.1524/ract.2002.90.4_2002.205
16. D. Rehe, A.Y. Kornienko, T.J. Emge et al., Thorium compounds with bonds to sulfur or selenium: synthesis, structure, and thermolysis. Inorg. Chem. **55**, 6961–6967 (2016). https://doi.org/10.1021/acs.inorgchem.6b00645
17. W. Wu, D. Rehe, P. Hrobárik et al., Molecular thorium compounds with dichalcogenide ligands: systhesis, structure, 77Se NMR study, and thermolysis. Inorg. Chem. **57**, 14821–14833 (2018). https://doi.org/10.1021/acs.inorgchem.8b02555

18. J.P. Perdew, K. Burke, M. Ernzerhof, Generalized gradient approximation made simple. Phys. Rev. Lett. **77**(18), 3865–3868 (1996). https://doi.org/10.1103/PhysRevLett.77.3865
19. A. Weigand, X.Y. Cao, T. Hangele et al., Relativistic small-core pseudopotentials for actinium, thorium, and protactinium. J. Phys. Chem. A **118**(13), 2519–2530 (2014). https://doi.org/10.1021/jp500215z
20. K.A. Peterson, Correlation consistent basis sets for actinides. I. The Th and U atoms. J. Chem. Phys. **142**(7), 074105 (2015). https://doi.org/10.1063/1.4907596
21. D.E. Woon, T.H. Dunning, Gaussian basis sets for use in correlated molecular calculations. III. The atoms aluminum through argon. J. Chem. Phys. **98**, 1358 (1993). https://doi.org/10.1063/1.464303
22. K.A. Peterson, D. Figgen, E. Goll et al., Systematically convergent basis sets with relativistic pseudopotentials. II. Small-core pseudopotentials and correlation consistent basis sets for the post-d group 16–18 elements. J. Chem. Phys. (2003). https://doi.org/10.1063/1.1622924
23. E.A. Dolgopolova, O.A. Ejegbavwo, C.R. Martin et al., Multifaceted modularity: a key for stepwise building of hierarchical complexity in actinide metal-organic frameworks. J. Am. Chem. Soc. **139**(46), 16852–16861 (2017). https://doi.org/10.1021/jacs.7b09496
24. Y.L. Li, J.H. Zou, X.G. Xiong et al., Probing chemical bonding and electronic structures in ThO^- by anion photoelectron imaging and theoretical calculations. J. Phys. Chem. A **121**, 2108–2113 (2017). https://doi.org/10.1021/acs.jpca.6b11554
25. Y.L. Li, J.H. Zou, X.G. Xiong et al., Anion photoelectron spectroscopy and chemical bonding of ThO_2^- and ThO_3^-. J. Chem. Phys. **148**, 244304 (2018). https://doi.org/10.1063/1.5030142
26. E.J. Baerends, T. Ziegler, J. Autschbach et al., ADF 2017.106, SCM, Theoretical Chemistry, Vrije Universiteit, Amsterdam, The Netherlands. http://www.scm.com
27. E. Van Lenthe, E.J. Baerends, Optimized Slater-type basis sets for the elements 1–118. J. Comput. Chem. **24**(9), 1142–1156 (2003). https://doi.org/10.1002/jcc.10255
28. E.D. Glendening, J.K. Badenhoop, A.E. Reed et al., Theoretical Chemistry Institute, University of Wisconsin, Madison, WI (2013). http://nbo6.chem.wisc.edu/
29. V. Goncharov, M.C. Heaven, Spectroscopy of the ground and low-lying excited states of ThO^+. J. Chem. Phys. **124**, 064312 (2006). https://doi.org/10.1063/1.2167356
30. L. Andrews, Y. Gong, B.Y. Liang et al., Matrix infrared spectra and theoretical studies of thorium oxide species: thO_x and Th_2O_y. J. Phys. Chem. A **115**, 14407–14416 (2011). https://doi.org/10.1021/jp208926m
31. A. Le, M.C. Heaven, T.C. Steimle, The permanent electric dipole moment of thorium sulfide. ThS. J. Chem. Phys. **140**, 024307 (2014). https://doi.org/10.1063/1.4861045
32. B. Liang, L. Andrews, Matrix infrared spectra and quasirelativistic DFT studies of ThS and ThS_2. J. Phys. Chem. A **106**(16), 4038–4041 (2002). https://doi.org/10.1021/jp014301m
33. L. Andrews, K.S. Thanthiriwatte, X.F. Wang et al., Thorium fluorides ThF, ThF_2, ThF_3, ThF_4, $ThF_3(F_2)$, and ThF_5^- characterized by infrared spectra in solid argon and electronic structure and vibrational frequency calculations. Inorg. Chem. **52**, 8228–8233 (2013). https://doi.org/10.1021/ic401107w
34. K.S. Thanthiriwatte, X.F. Wang, L. Andrews et al., Properties of ThF_x from infrared spectra in solid argon and neon with supporting electronic structure and thermochemical calculations. J. Phys. Chem. A **118**, 2107–2119 (2014). https://doi.org/10.1021/jp412818r
35. H.-J. Werner, P.J. Knowles, G. Knizia et al., M. MOLPRO, Version 2012.1, A Package of ab Initio Programs. http://www.molpro.net
36. P. Pyykkö, S. Riedel, M. Patzschke, Triple-bond covalent radii. Chem. Eur. J. **11**, 3511–3520 (2005). https://doi.org/10.1002/chem.200401299